Monthly Notices
of the
ROYAL ASTRONOMICAL SOCIETY

Mon. Not. R. Astron. Soc. **415,** 2910–2919 (2011) doi:10.1111/j.1365-2966.2011.18904.x

Testing black hole jet scaling relations in low-luminosity active galactic nuclei

F. de Gasperin,[1,2⋆] A. Merloni,[2,3] P. Sell,[4] P. Best,[5] S. Heinz[4] and G. Kauffmann[1]

[1]*Max-Planck-Institut für Astrophysik, Karl-Schwarzschild-Str. 1, D-85741 Garching, Germany*
[2]*Exzellenzcluster Universe, Boltzmann-Str. 2, D-85748 Garching, Germany*
[3]*Max-Planck-Institut für Extraterrestrische Physik, Giessenbachstr., D-85741 Garching, Germany*
[4]*University of Wisconsin-Madison, 475 North Charter Street, Madison, WI 53706, USA*
[5]*Institute for Astronomy, University of Edinburgh, Blackford Hill, EH9 3HJ Edinburgh*

Accepted 2011 April 12. Received 2011 April 4; in original form 2011 January 10

ABSTRACT

We present the results of the analysis of a sample of 17 low-luminosity ($L_X \lesssim 10^{42}$ erg s^{-1}), radio-loud active galactic nuclei in massive galaxies. The sample is extracted from the Sloan Digital Sky Survey data base and it spans uniformly a wide range in optical [O III] emission line and radio luminosity, but within a narrow redshift range ($0.05 < z < 0.11$) and a narrow supermassive black hole mass range ($\sim 10^8$ M$_\odot$). For these sources we measured core X-ray emission with the *Chandra X-ray Telescope* and radio emission with the Very Large Array. Our main goal is to establish which emission component, if any, can be regarded as the most reliable accretion/jet-power estimator at these regimes. In order to do so, we studied the correlation between emission-line properties, radio luminosity, radio spectral slopes and X-ray luminosity, as well as more complex multivariate relations involving black hole mass, such as the Fundamental Plane of black hole activity. We find that 15 out of 17 sources of our sample can be classified as low-excitation galaxies (LEGs), and their observed properties suggest X-ray and radio emission to originate from the jet basis. We also find that X-ray emission does not appear to be affected by nuclear obscuration and can be used as a reliable jet-power estimator. More generally, X-ray, radio and optical emission appear to be related, although no tight correlation is found. In accordance with a number of recent studies of this class of objects, these findings may be explained by a lack of cold (molecular) gaseous structures in the innermost region of these massive galaxies.

Key words: galaxies: active – galaxies: jets – galaxies: nuclei.

1 INTRODUCTION

In this work we focus on three accretion/jet-power estimators among the different signatures of galactic nuclear activity arising at different wavelengths: optical line emission, nuclear X-rays and nuclear non-thermal radio emission. In the standard 'unified model' for active galactic nuclei (AGN; Urry & Padovani 1995), optical narrow emission lines come from gas located several hundreds pc away from the central engine. These lines are excited by ionizing radiation produced in the innermost accretion flow and escaping along the polar axis of the obscuring torus that surrounds the black hole. Since this ionized gas is so distant from the central engine, the obscuring torus does not affect greatly its flux; thus, narrow optical emission lines suffer only moderate amounts of dust obscuration due to the interstellar medium (ISM). This suggests that [O III] emission-line luminosity can be a good estimator for the AGN accretion power. On the contrary, X-ray emission arises directly from the hot corona surrounding the accretion disc or from the base of a relativistic jet (for radio-loud objects). As such, it represents a more faithful estimator of the accretion power, although it could be heavily obscured by high column density through the dusty torus in objects where we look at the AGN from a close to edge-on sightline. Finally, powerful non-thermal radio emission is the observational signature of the presence of a jet whose relativistic particles emit synchrotron radiation going through strong magnetic fields. Radio-emitting jets are ubiquitous, particularly at low intrinsic powers (see e.g. Ho 2008, and references therein), and it has been postulated that it also could be used to estimate the AGN kinetic and total power output (Falcke & Biermann 1995; Best et al. 2006).

⋆E-mail: fdg@mpa-garching.mpg.de

As emerged in recent years (see Hardcastle, Evans & Croston 2009, and references therein), radio-loud objects can be divided into two main populations.

(i) *High-excitation galaxies* (*HEGs*). Quasars and high-power narrow-line radio galaxies that are likely to be the same population, seen at different orientations.

(ii) *Low-excitation galaxies* (*LEGs*). Active radio galaxies of low intrinsic power characterized by emission-line spectra of low excitation, which probably form the parent population of the mostly lineless BL Lac objects.

Recent studies (Chiaberge, Capetti & Celotti 2002; Whysong & Antonucci 2004; Evans et al. 2006; Hardcastle, Evans & Croston 2006; Hardcastle et al. 2009) have proposed that LEGs lack any of the conventional apparatus of the AGN (i.e. radiatively efficient accretion disc, X-ray corona and obscuring torus) and that their radio and X-ray nuclear emission can be explained as a result of the properties of the small-scale jet.

Significant progress has also been achieved in understanding how the radio properties of AGN relate to other parameters such as black hole mass and accretion rate (Ho 2002). Merloni et al. (2003, hereafter M03) and Falcke, Koerding & Markoff (2004) considered heterogeneous black hole samples spanning a broad range in black hole mass and X-ray luminosity, and found a strong correlation between the radio luminosity $L_{\rm R}$ from the unresolved radio cores of AGN, the black hole mass M and the 2–10 keV X-ray luminosity $L_{\rm X}$ of the form (M03)

$$\log L_{\rm R} = 7.44 + 0.6 \log L_{\rm X} + 0.78 \log(M/{\rm M}_{\odot}). \quad (1)$$

These scalings with mass and luminosity can be well explained by the theory of synchrotron-emitting compact relativistic jets and radiatively inefficient accretion flows (Blandford & Konigl 1979; Heinz & Sunyaev 2003). These works explicitly demonstrated that the black hole mass should be considered as a fundamental parameter in the determination of the observed relations between emission components in various bands.

In this paper we want to push forward these investigations on the relations between different accretion and power output estimators in supermassive black hole (SMBH). In particular, we will test whether the loose empirical [O III]–X-ray correlation found in type 1 AGN, as well as the Fundamental Plane of black hole activity, holds in an unbiased sample of type 2 AGN in the local universe. Compared to previous work on this subject (see e.g. Heckman et al. 2005, hereafter H05), this study is unique because we select objects in a very narrow range of black hole masses, thus disentangling the effects of mass and accretion rate on the observed [O III]–X-ray–radio correlations.

The paper is organized as follows. In Section 2 we describe our sample, while in Section 3 we lay out the most important calibration steps used for the X-ray, radio and optical data reduction. Then in Section 4 we examine the relation between different power estimators. Finally in Section 5 we discuss their implications.

2 SAMPLE SELECTION

In order to answer some of the important questions posed in the previous section, we have performed a snapshot X-ray/radio survey of a new, well-defined sample of low-luminosity AGN (LLAGN). The sample used for our analysis was originally extracted from 2712 radio luminous type 2 AGN (Best et al. 2005) contained in the 212 000 galaxies of the second data release (DR2) of the Sloan Digital Sky Survey (SDSS). From this sample we selected 17 objects with the following characteristics.

(i) The black hole masses have been derived from velocity dispersion measurements of each galaxy (Tremaine et al. 2002; Heckman et al. 2004). We require black hole masses to be $8 \leq \log M_{\rm BH} \leq 8.5$ (the range is comparable to the uncertainty in the estimate of $M_{\rm BH}$). This particular window was chosen to maximize the number of objects with $z \leq 0.11$ that are radio loud.

(ii) A second cut was made on the redshift: $0.05 \leq z \leq 0.11$. The SDSS spectra are obtained using 3-arcsec-diameter fibres and at larger distances, and the AGN emission is significantly contaminated by starlight from the host galaxy.

(iii) The objects were chosen to span a wide range in dust-corrected [O III] luminosity ($L_{[\rm O\,III]} \sim 10^{5.5}\,{\rm L}_{\odot}$ up to $L_{[\rm O\,III]} = 10^{9.2}\,{\rm L}_{\odot}$), and the entire observed range in radio luminosity, $10^{38.5}\,{\rm erg\,s^{-1}} \leq L_{\rm R} \leq 10^{41.3}\,{\rm erg\,s^{-1}}$.

(iv) In order to not be biased by cluster environment and to facilitate the X-ray data reduction, we chose objects that were at least 7 arcmin away from the centre of galaxy clusters.

142 AGN satisfy all these conditions. Because of their intrinsic weakness, a full multiwavelength survey of the entire sample was deemed too time consuming. Instead, we chose to focus on a randomly selected subsample of 17 objects to cover the $L_{[\rm O\,III]}$–$L_{\rm R}$ parameter space widely. The final choice of the sample size was made by trading off the total observing time requested for maximizing the chances of source detection in the X-rays and ensuring that enough sources are included for statistical tests.

Properties of the galaxies in the selected sample are listed in Table 1, while in Fig. 1 we plot the sample on the [O III]–radio plane using line luminosities from SDSS DR 7. At the time of the sample selection the last SDSS release available was the fourth. Subsequent analyses and better calibration of the SDSS spectroscopic data imply that some [O III] luminosity values differ slightly between the two releases due to different data-reduction procedures, and this is the reason why two objects (9 and 17) are quite near in the [O III]–radio plane, while, as stated above, we selected them to cover that space as uniformly as possible. Finally, we stress that in the sample-selection process we did not exclude any source on the basis of the ionization state of the emission-line complex, so that no bias for or against the HEG/LEG nature of the sources had been introduced. After our observations were taken, Plotkin et al. (2008), using radio and optical data, have classified one of them as a BL Lac with a strong boosting in the radio and X-ray emission. This is source number 4 in Table 1, and is a clear outlier in most of the diagrams presented throughout the paper. We decided to leave it in the sample for completeness of information.

Throughout this paper, luminosity distances are calculated adopting $H_0 = 70\,{\rm km\,s^{-1}\,Mpc^{-1}}$, $\Omega_{\rm m} = 0.3$ and $\Omega_{\Lambda} = 0.7$.

3 DATA ANALYSIS

Our sample of 17 objects has been observed with *Chandra X-ray Telescope* (see Section 3.1) and with the Very Large Array (VLA; see Section 3.2). Information about their [O III] luminosities is taken from the SDSS and is analysed as explained in Section 3.3.

All errors due to inaccurate evaluation of distances are considered negligible, while we account for an error of 0.25 dex in the black hole mass (Tremaine et al. 2002). Throughout the paper, linear fits have been performed using the Buckley–James method (Buckley & James 1979; Isobe, Feigelson & Nelson 1986) to account for upper limits. With this regression algorithm, the most probable values

Table 1. The sample.

Object	ID	RA J2000	Dec. J2000	z	$\log L_{[\mathrm{O\,III}]}$	$\log L_{\mathrm{X}}$ 2–10 keV	1.4 GHz	$\log L_{\mathrm{R}}$ 4.8 GHz	8.4 GHz	α_{R}	$\log M_{\mathrm{BH}}$
(1)	(2)			(3)	(4)	(5)	(6)	(7)	(8)	(9)	(10)
2MAS1601+46	1	16:01:09.07	46:23:17.8	0.08	40.0 ± 0.13	$41.0^{+0.34}_{-0.84}$	38.6	39.2	39.4	0.12	8.0
2MAS0837+53	2	08:37:17.99	53:15:16.8	0.06	40.2 ± 0.08	<41.5	39.0	39.9	40.1	−0.08	8.3
2MAS1349+05	3	13:49:07.22	05:04:12.1	0.08	39.2 ± 0.30	$41.0^{+0.38}_{-0.34}$	39.4	39.7	39.9	0.23	8.0
CGCG043−05	4	12:53:47.01	03:26:30.4	0.07	39.9 ± 0.07	$43.2^{+0.20}_{-0.17}$	40.1	40.6	40.8	0.17	8.5
SDSS0141−09	5	01:41:16.35	−08:35:39.3	0.05	39.9 ± 0.04	<41.0	38.9	39.4	39.6	0.05	8.0
2MAS1612+00	6	16:12:09.29	00:03:33.1	0.06	40.1 ± 0.06	$41.3^{+0.18}_{-0.88}$	39.3	40.0	40.2	0.16	8.4
SDSS2122−08	7	21:25:12.48	−07:13:29.9	0.06	41.1 ± 0.01	$42.3^{+0.11}_{-0.13}$	38.7	38.9	39.2	−0.13	8.3
2MAS1109+02	8	11:09:57.14	02:01:38.6	0.06	41.7 ± 0.00	$42.6^{+0.67}_{-0.76}$	38.9	39.1	39.1	0.94	8.0
2MAS0836+53	9	08:36:42.83	53:34:32.5	0.10	40.6 ± 0.03	$41.7^{+0.20}_{-0.23}$	39.8	40.6	40.8	0.08	8.5
2MAS1349+04	10	13:49:09.63	04:04:48.3	0.08	41.1 ± 0.04	$40.4^{+0.70}_{-1.19}$	40.2	40.2	40.2	1.04	8.3
2MAS0912+53	11	09:12:01.68	53:20:36.6	0.10	41.4 ± 0.01	$41.2^{+0.32}_{-0.60}$	40.7	41.0	41.2	0.41	8.3
2MAS0810+48	12	08:10:40.28	48:12:33.2	0.08	42.4 ± 0.01	$41.1^{+0.72}_{-0.33}$	40.1	40.2	40.2	0.94	8.1
2MAS1542+52	13	15:42:28.36	52:59:50.9	0.07	41.0 ± 0.03	$42.0^{+0.37}_{-0.32}$	39.6	40.1	40.6	−1.14	8.5
4C52.370	14	16:02:46.39	52:43:58.4	0.11	41.8 ± 0.03	$41.7^{+0.31}_{-0.37}$	41.4	41.5	41.5	0.94	8.5
LCRS1010−02	15	10:12:39.87	−01:06:22.9	0.10	41.4 ± 0.03	$41.1^{+0.63}_{-0.39}$	39.4	39.9	40.1	0.32	8.2
2MAS0101−00	16	01:01:01.11	−00:24:44.4	0.10	41.0 ± 0.02	$40.9^{+0.34}_{-1.00}$	39.3	39.7	39.8	0.72	8.4
SDSS2305−10[a]	17	23:08:17.29	−09:46:22.5	0.10	40.6 ± 0.07	$41.3^{+0.28}_{-0.25}$	39.8	40.1	40.4	0.10	8.3

Note. Column (1): name of the object. Column (2): identification number. Column (3): redshift. Column (4): [O III] luminosity $\log(L_{[\mathrm{O\,III}]}[\mathrm{erg\,s^{-1}}])$ corrected for dust absorption. Column (5): X-ray luminosity $\log(L_{\mathrm{X}}[\mathrm{erg\,s^{-1}}])$ (corrected for absorption). Column (6): radio luminosity at 1.4 GHz $\log(L_{1.4}[\mathrm{erg\,s^{-1}}])$. Column (7): radio luminosity at 4.8 GHz $\log(L_{4.8}[\mathrm{erg\,s^{-1}}])$ (mean 5σ error: 0.023 dex). Column (8): radio luminosity at 8.4 GHz $\log(L_{8.4}[\mathrm{erg\,s^{-1}}])$ (mean 5σ error: 0.024 dex). Column (9): radio spectral index, defined with $F \propto \nu^{-\alpha}$. Column (10): SMBH mass $\log(M[\mathrm{M}_{\odot}])$.
[a]Resolved in the radio maps.

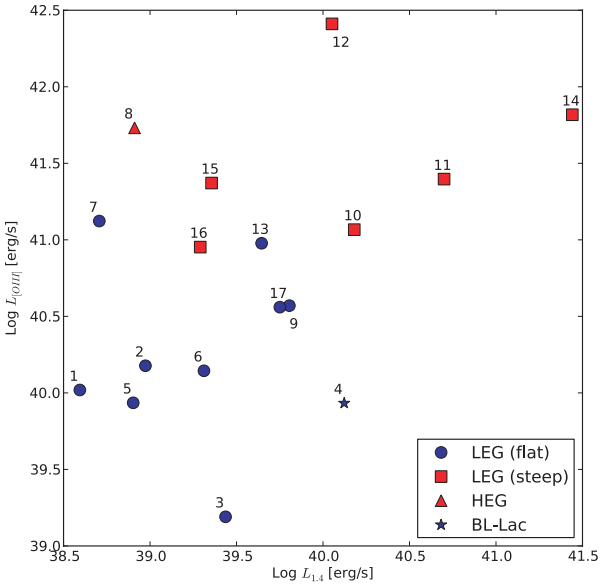

Figure 1. Sources in our sample plotted in a radio (1.4 GHz)–optical ([O III]) luminosity plane. Sources are selected in order to cover wide range of luminosity both in the radio and the optical. Points are coloured according to their spectral index in the radio band (red: steep-spectrum; blue: flat-spectrum, see Section 3.2 for details). Square markers are for LEG steep-spectrum objects, round markers are for LEG flat-spectrum objects, while the triangle marker is the HEG and the star marker is the BL Lac. For the classification criteria see Sections 3.2 and 3.3.

of the upper limits are evaluated through the Kaplan–Meier non-parametric distribution (Kaplan & Meier 1958) and then used as observed values for a linear fit that is performed using the orthogonal distance regression to take into account errors both in the dependent and in the independent variable. Correlation tests were performed using a generalized Kendall correlation test (Isobe et al. 1986) that accounts also for upper limits and, if needed, for partial correlation (Akritas & Siebert 1996).

3.1 X-ray

All of the AGN were observed on the S3 chip of the Advanced CCD Imaging Spectrometer (ACIS; Garmire et al. 2003) aboard the *Chandra X-ray Observatory*. Data were taken in timed exposure mode with the standard frame time at the default location on the S3 chip and telemetered to the ground in very faint mode. Data reduction and point source extractions were completed using CIAO versions 4.2, and ACIS EXTRACT version 2010-02-26 (AE; Broos et al. 2010), respectively. During extraction, the source position was adjusted based on the mean position of the extracted counts to more accurately calculate the point source photometry (except for the two sources with upper limits). The position refinement was always well within *Chandra*'s absolute position uncertainty.

We used SHERPA version 4.2 to jointly fit the unbinned source and background spectrum of each source (Freeman, Doe & Siemiginowska 2001) using the *C*-statistic, which is similar to the Cash (1979) statistic but with an approximate goodness-of-fit measure, and the MONCAR[1] minimization algorithm. We used this statistical

[1] http://cxc.harvard.edu/sherpa4.2/ahelp/montecarlo.py.html

Table 2. X-ray data analysis values.

ID (1)	ID *Chandra* (2)	Obs. date	Exposure time (s)	Source counts (3)	Exp. bkg counts (4)	Photon index (5)	$N_{\rm H}$ (10^{22} cm^{-2}) (6)	Probability no source (7)
1	8244	2008-01-16	11 629	12	0.07	1.70	$1.33^{+14.3}_{-1.33} \times 10^{-2}$ [a]	4.93×10^{-23}
2	8245	2007-09-30	6938	2	0.06	1.70	3.51×10^{-2} [b]	1.52×10^{-03}
3	8246	2007-03-15	10 888	29	0.06	$2.31^{+1.85}_{-0.35}$	$1.99^{+42.2}_{-1.99} \times 10^{-2}$ [a]	0.00
4	8247	2007-03-04	8021	1044	0.10	$2.53^{+1.14}_{-0.37}$	$6.25^{+11.5}_{-5.19} \times 10^{-2}$	0.00
5	8248	2007-10-03	5109	2	0.03	1.70	3.04×10^{-2} [b]	3.47×10^{-4}
6	8249	2007-04-11	5950	22	0.04	1.70	$7.42^{+16.4}_{-7.42} \times 10^{-2}$ [a]	0.00
7	8250	2007-06-29	6880	260	0.05	$1.68^{+0.21}_{-0.16}$	$6.00^{+6.65}_{-6.00} \times 10^{-2}$	0.00
8	8251	2007-04-10	6938	15	0.04	1.70	$33.3^{+14.7}_{-17.9}$	2.87×10^{-30}
9	8252	2006-12-16	15 933	101	0.13	$2.23^{+0.28}_{-0.19}$	$3.58^{+6.67}_{-3.58} \times 10^{-2}$ [a]	0.00
10	8253	2007-03-07	11 005	3	0.06	1.70	1.97×10^{-2} [b]	3.09×10^{-05}
11	8254	2007-06-07	18 782	21	0.15	1.70	$1.78^{+14.5}_{-1.78} \times 10^{-2}$ [a]	3.32×10^{-37}
12	8255	2007-10-08	11 008	12	0.07	1.70	$1.67^{+3.12}_{-1.67} \times 10^{-1}$	7.36×10^{-23}
13	8256	2007-06-04	8912	20	0.05	1.70	$4.25^{+1.99}_{-1.26}$	1.96×10^{-44}
14	8257	2007-06-03	19 911	30	0.13	$1.34^{+1.10}_{-0.47}$	$1.14^{+4.72}_{-1.14} \times 10^{-1}$	0.00
15	8258	2007-01-13	16 940	10	0.09	1.70	$3.99^{+7.53}_{-3.99} \times 10^{-1}$	1.88×10^{-17}
16	8259	2008-02-09	16 808	8	0.13	1.70	$3.17^{+41.6}_{-3.17} \times 10^{-2}$ [a]	1.97×10^{-12}
17	8260	2007-10-20	17 934	59	0.11	$2.42^{+0.27}_{-0.26}$	$3.09^{+2.60}_{-3.09} \times 10^{-2}$ [a]	0.00

Note. Column (1): identification number. Column (2): identification number used in *Chandra* observations. Column (3): number of source counts (0.5–8 keV) in the 90 per cent point spread function. Column (4): expected background counts in source region (0.5–8 keV). Column (5): the best fits for the photon index and relative upper/lower limit increments. When the value is frozen to 1.7 (see text for details) the upper and lower limits are not calculable and therefore omitted. Column (6): the column densities $N_{\rm H}$ and relative upper/lower limit increments. Column (7): 'prob_no_source' value, defined in section 5.10.3 of the AE user manual (http://www.astro.psu.edu/xray/docs/TARA/ae_users_guide/). SHERPA's 'conf' routine has been used to calculate the uncertainties in the photon index and column density (columns 5 and 6). SHERPA's 'conf' method gives similar uncertainties to the grid method used in the calculation of the uncertainty in the luminosity, except that SHERPA's 'conf' routine tends to underestimate the uncertainty relative to the grid method (e.g. on the order of a few tens of percent for the photon index).

[a] Indicates that the best fit happens to be at the galactic minimum.

[b] Indicates that $N_{\rm H}$ is frozen to the galactic minimum.

method for the fitting to avoid losing the little spectral information that we have for most of our spectra, which frequently have very few counts (e.g. Nousek & Shue 1989). We fitted each source with an absorbed power-law model (XSZPHABS × XSPOWERLAW). In all cases, the background exhibited the signs of hard particle background and was fitted by two power laws and thermal component, which achieved a good fit. These ad hoc models are only used to constrain the background component of the spectra.

Since degeneracies in the fit parameters will frequently arise for very faint sources, we followed a specialized scheme for these sources based on the number of counts in the source extraction region. If we extracted less than five counts (0.5–8 keV) for a source, the power-law index and the hydrogen column density for the fit were frozen to 1.7 and the Galactic value, respectively. If we extracted more than 5 but less than 26 count (0.5–8 keV), we froze only the power-law index to 1.7 and let the hydrogen column density float, although, in this case, it was always poorly constrained. For all other sources with more than 26 count (0.5–8 keV), we allowed all fit parameters to float.

As can be seen in Table 2, the AGN span a wide range of brightness. We put upper limits on the luminosities of two of the sources with only two counts each (identified with numbers 2 and 5 in Table 1). On the other hand, there were also two sources (IDs 4 and 7 in Table 1) that had non-negligible pile-up fractions[2] (39.3 and 4.6 per cent of the counts, respectively) and were therefore fitted with the standard pile-up model. Only two sources (number 8 and, to a lesser amount, 13) have significant additional intrinsic absorption above that expected for the galactic foreground (Dickey & Lockman 1990). However, the determination of the column density for all of our sources is highly uncertain.

The unabsorbed X-ray luminosities listed in Table 1 were calculated from each of the model fits and the uncertainties were calculated as follows. The unabsorbed luminosity is evaluated at each point in a three-dimensional grid 100 points on a side, each dimension corresponding to the number of undetermined parameters in the source model (the absorption, power-law photon index and power-law normalization). Then the minimum and maximum luminosity is selected within the confidence interval for the appropriate change in statistic value ($\Delta C = 3.53$ for 1σ and three interesting parameters; e.g. Avni 1976). The photon index is constrained to be 0.7–2.7 and the column density must be at least the galactic minimum in the direction of the source. In many cases, the uncertainties in the luminosity estimated with this method are very different from those

[2] http://cxc.harvard.edu/ciao/ahelp/acis_pileup.html

estimated from the counts using Bayesian methods (Kraft, Burrows & Nousek 1991).

Finally, we note that, since the *Chandra* observations were carried out over the span of 1 yr (late 2006 to early 2008), variability between the time of X-ray observations and radio observations could affect some of our results.

3.2 Radio

Radio data were taken in 2007 using the VLA in A configuration with a total observation time of 10 h. The calibration procedure has been performed using CASA software (version 3.0.1) developed at NRAO.[3] At the time of the observations, 12 out of 26 antennas were already equipped with EVLA receivers. The presence of two different types of receivers on the antennas caused different response from the correlator whether a mixed baseline (VLA–EVLA) or a non-mixed one (VLA–VLA and EVLA–EVLA) was processed. To solve the problem, a baseline-based calibration was performed using the CASA task BLCAL. Finally, some cycles of self-calibration have been done on all sources.

We observed our sample in two different bands (4.8 and 8.4 GHz), and from these flux values radio spectral indices have been extracted. Sources with a spectral index ($F \propto \nu^{-\alpha}$) higher than $\alpha = 0.3$ are classified as steep spectrum, while other sources are classified as flat spectrum. Values from the FIRST survey (1.4 GHz) were not taken into account during the spectral index extraction process because source fluxes could have changed since FIRST observations. From the spectral analysis, we find that 10 out of 17 sources of our sample have a flat spectrum, while in one case (source 13), the spectrum is inverted.

To check the radio calibration procedure, we computed the spectral index average values using the three different bands (1.4, 4.8 and 8.4 GHz) two by two. If the main driver for changes in the spectral shape between any two bands is time variability, then some of the sources would have an increased spectral index while some other a lowered one, with an average value of zero. This means that the three averaged spectral index values should be similar. We find an averaged spectral index $\alpha_{4.8-8.4} = -0.29 \pm 0.12$ between 4.8 and 8.4 GHz, $\alpha_{1.4-4.8} = -0.24 \pm 0.10$ between 1.4 and 4.8 GHz and $\alpha_{1.4-8.4} = -0.25 \pm 0.09$ between 1.4 and 8.4 GHz. They are all compatible, enforcing the idea that individual differences between spectral indices including the low-frequency FIRST observations are mostly due to time variability.

The sample was selected to be unresolved at the FIRST resolution (5 arcsec), and only one source (number 17) shows clear evidence of a resolved structure in our new observations, which is a 1-arcsec-long, jet-like feature in the west–north-west direction. Finally, radio fluxes were corrected so that all of them will be at the same rest-frame frequency using the derived spectral indices. Errors on radio fluxes have been set to fives times the background rms obtained analysing the final maps.

3.3 Optical

We have re-analysed the available SDSS spectra for the sources in our sample in order to assess the physical nature of the emission lines. Optical spectroscopic information plays a major role in understanding emission properties of central engine of radio galaxies. A first classification using spectral lines was made by Heckman (1980) and Baldwin, Phillips & Terlevich (1981). They proposed to use optical line ratios to distinguish between H II regions ionized by star-forming activities and regions ionized by AGN. Some years later, Veilleux & Osterbrock (1987) revised these definitions using only ratios of lines with a small separation in wavelength, in order to reduce the reddening problem and the impact of flux calibration errors. They introduced these lines combinations: [O III] λ5007/Hβ, [N II] λ6583/Hα, [S II] $\lambda\lambda$6716, 6731/Hα and [O I] λ6364/Hα. The separation between AGN and H II regions was also calibrated by Kewley et al. (2001) and again by Kewley et al. (2006) using ~85 000 emission-line galaxies from the SDSS catalogue. Seyfert and LINERs occupy in these diagnostic diagrams different places, and the authors suggested that the observed dichotomy corresponds to two AGN subpopulations associated with different accretion modes.

Attempts to apply these diagnostic diagrams to radio-loud galaxies were made by Laing et al. (1994) on a subsample of 3CR radio galaxies. Following the suggestion by Hine & Longair (1979) that Fanaroff–Riley type II (FR II) sources can be divided into two subclasses, they separated their sample into HEGs (defined as galaxies with [O III]/H$\alpha > 0.2$ and equivalent width of [O III] > 3 Å) and LEGs. Following this idea, we have divided our radio-loud sample in HEGs and LEGs using the criteria described in Buttiglione et al. (2009), where they take advantage from the combination of the optical diagnostic planes. They define LEGs as all the sources with $\log([\mathrm{O\,III}]/\mathrm{H}\beta) - [\log([\mathrm{N\,II}]/\mathrm{H}\alpha) + \log([\mathrm{S\,II}]/\mathrm{H}\alpha) + \log([\mathrm{O\,I}]/\mathrm{H}\alpha)]/3 < 0.95$.

We calculated lines luminosities using the spectra extracted from the SDSS DR 7 (Abazajian et al. 2009). For our purposes we are interested both in the [O III] observed line fluxes and in the dust-corrected line fluxes. When dust attenuation needs to be taken into account we measure Hα and Hβ line intensities and use the Balmer decrement method. We assume an intrinsic Hα/Hβ of 2.87 (Osterbrock 1989). The attenuation correction we use is a double power law (Charlot & Fall 2000) of the form

$$\frac{\tau_\lambda}{\tau_\nu} = (1-\mu)\left(\frac{\lambda}{5500\ \text{Å}}\right)^{-1.3} + \mu\left(\frac{\lambda}{5500\ \text{Å}}\right)^{-0.7}, \quad (2)$$

where τ_ν is the total effective optical depth in the V band. With this double power law, we account for the attenuation due the presence of discrete clouds random distributed (first term) and the attenuation due to the ISM (second term), so μ is the fraction of total τ_ν caused by ambient ISM. We set $\mu = 0.3$ based on observed relations between UV continuum slope and the Hα-to-Hβ line ratios.

We have generated emission-line diagnostic (Baldwin et al. 1981) diagrams to compare emission-line ratios ([O III] λ5007/Hβ, [O I] λ6003/Hα, [S II] λ6717, 7631/Hα and [N II] λ6584/Hα) of our sample (see Fig. 2).

Following the previously explained classification from Buttiglione et al. (2009), we can classify the majority of our sources as LEGs and be confident only for source 8 to be classified as an HEG. Some sources (11 and 12) fall in an intermediate position since they do not satisfy the required line luminosity ratios in all diagnostic diagrams and they are then classified as LEGs. We must note that with this division all sources optically classified as LINERs are now classified as LEGs, and source number 8, optically classified as a Seyfert, is an HEG. The difference in the classifications is mainly for borderline objects (in our sample: 11, 12 and 16) that are conventionally classified as Seyfert galaxies but in Buttiglione et al. (2009) classification are instead LEGs (see Fig. 2). Contrary to what was found by Buttiglione et al. (2009), we have some strong [O III] emitters ($L_{[\mathrm{O\,III}]} > 10^{41.5}$) that do not have $\log$ [O III]/H$\beta \sim 1$,

[3] http://casa.nrao.edu/

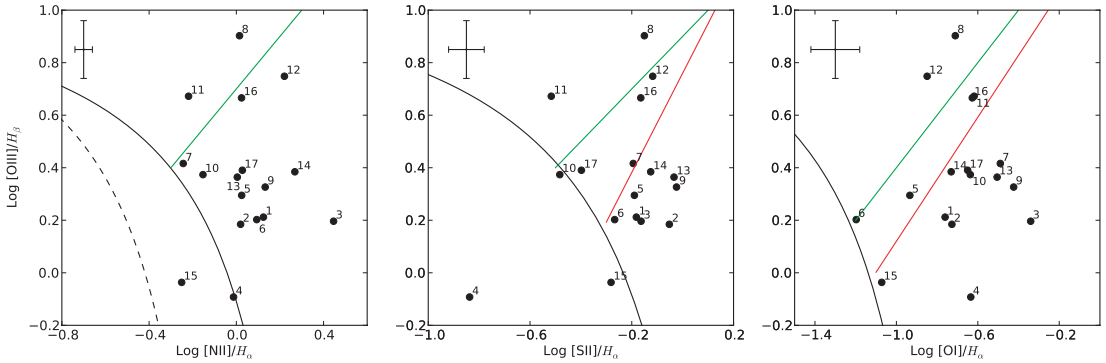

Figure 2. Diagnostic diagrams for our 17 sources. Black solid lines (Kewley et al. 2006) separate star-forming galaxies, on the bottom left of each diagram, from AGN. The region between dashed and solid lines (Kewley et al. 2006) identify *composite galaxies* with both star-forming and AGN activities. Red lines (Kewley et al. 2006) separate Seyfert galaxies (above) from LINERs (below). Green lines (Buttiglione et al. 2009) separate HEG (top) from LEG (bottom) sources. Average error bars are shown in the top left-hand corner of each plot.

but lower values, e.g. source 12 and 14. Finally, object number 4 is an outlier in many plots. The reason is that this source, as classified by Plotkin et al. (2008) using radio and optical data, is a BL Lac with a strong boosting in the radio and X-ray emission.

4 COMPARISON AMONG [O III], X-RAY AND RADIO PROPERTIES

In this section we analyse the correlations and properties that connect [O III], X-ray and radio emissions from the sample of sources described in Section 2. As a preliminary step, we have performed a partial correlation analysis on the sample (and various subsamples), both for the observed luminosities and for those corrected for absorption/extinction, as discussed in the previous section. We adopt the Akritas & Siebert (1996) method to control for censored data. Table 3 shows a summary of such a study, where the presence of a correlation between two variables is tested accounting for the common dependence on the third (test variable). In the next sections, relations between different accretion power estimators are evaluated and discussed in detail: in Section 4.1 we present the analysis of the relationship between [O III] and X-ray emission in our sample, while in Section 4.2 we exploit the knowledge of radio spectra to provide an interpretation of the X-ray and [O III] information. Finally, in Section 4.3 we discuss the X-ray–radio correlation (or lack of it) in light of previous studies on the Fundamental Plane of active black holes.

Table 3. Partial correlation coefficients.

Indep. variable	Dep. variable	Test variable	Prob. of non-correlation Observed	Corrected
		All sample		
X-ray	Radio	[O III]	0.93	0.98
Radio	[O III]	X-ray	0.29	0.06
[O III]	X-ray	Radio	**0.01**	0.09
		LEG		
X-ray	Radio	[O III]	0.60	0.48
Radio	[O III]	X-ray	0.12	<**0.01**
[O III]	X-ray	Radio	0.23	0.44
		Radio steep-spectrum sources		
X-ray	Radio	[O III]	0.38	0.82
Radio	[O III]	X-ray	0.22	**0.02**
[O III]	X-ray	Radio	<**0.01**	0.09
		Radio flat-spectrum sources		
X-ray	Radio	[O III]	0.45	0.48
Radio	[O III]	X-ray	0.87	0.88
[O III]	X-ray	Radio	**0.05**	**0.05**

Note. In boldface are those values where the significance is ≥95 per cent.
Object number 4 is not considered.

4.1 Accretion estimators: the relationship between [O III] and X-ray emission

In H05 the authors emphasized the strong difference that arises if one considers AGN samples of Seyfert galaxies selected by X-ray luminosity or using the [O III] line luminosity. For a sample of hard X-ray-selected AGN (flux limit in the 3–20 keV band of 2.5×10^{-11} erg s^{-1} cm^{-2}), they find a mean $\log(L_X/L_{[O\,III]})$ of 2.15 dex and $\sigma = 0.51$ dex. Type 1 and type 2 sources are separated in terms of emission intensities, but do not present significant difference in the mean ratio between X-ray and [O III] luminosities. In the left-hand panel of Fig. 3, the H05 X-ray-selected data set is shown together with our sample, without applying any absorption/extinction corrections, for ease of comparison (absorption-corrected correlations are discussed in the following sections). Sources in our sample have a systematically lower X-ray-to-[O III] ratio (see Table 4); this is in agreement with the different selection criteria used for the two samples. In the H05 X-ray-selected sample, a higher X-ray emission is indeed expected.

In the right-hand panel of Fig. 3, we compare instead our data set with the [O III]-selected sample of H05 ([O III] λ5007 fluxes greater than 2.5×10^{-13} erg cm^{-2} s^{-1}, corresponding to $L_{[O\,III]} \gtrsim 10^{40}$ erg s^{-1}). As noted by H05, type 1 AGN are detected at the expected rate, while around two-third of the type 2 AGN would have been missed by the X-ray selection criteria. Their conclusion is that the missing type 2 AGN are almost certainly heavily X-ray absorbed. Our sample shows a different behaviour. Our objects in fact do not show a random scatter in X-ray luminosity for a given [O III] line luminosity; they rather are quite aligned with the H05 [O III]-selected type 1 sample. This can be quantified in terms of the average luminosity ratios of the samples: in H05, [O III]-selected type 2 AGN have an average $\log(L_X/L_{[O\,III]})$ of 0.57 with a σ of 1.06 dex. Our sample has instead a higher X-ray-to-[O III] average ratio of 1.25 dex with a much smaller σ of 0.57 dex. Interestingly, this relation is much more similar to what H05 find for the

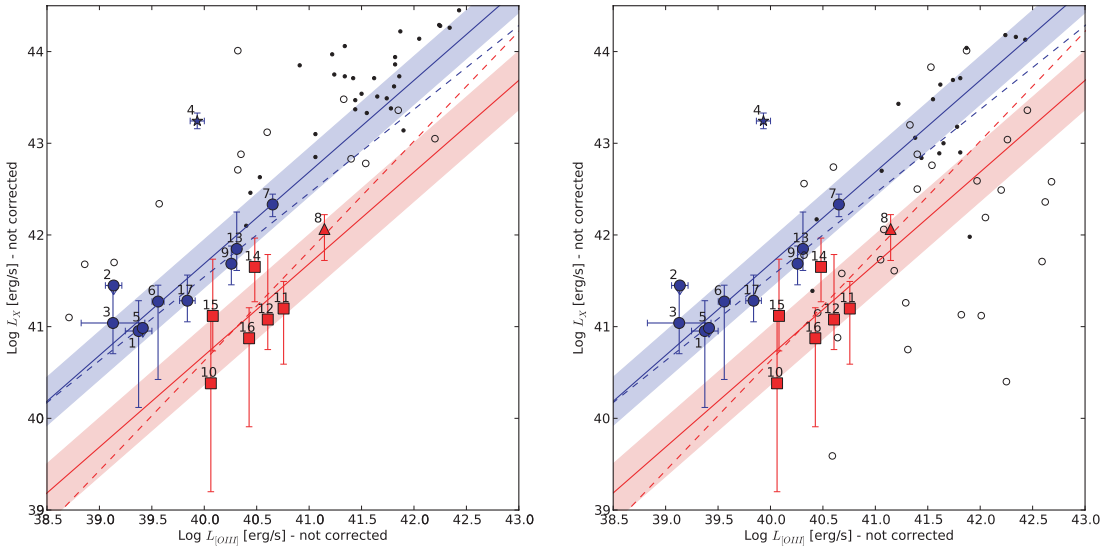

Figure 3. Left-hand panel: our sample on an X-ray [2–10 keV]–optical ([O III]) plane (uncorrected for absorption). Symbols are as in Fig. 1. Black dots are type 1 objects from H05 hard X-ray-selected sample, while circles are type 2 objects. Red and blue solid lines are the mean ratio between $\log L_X$ and $\log L_{[O\,III]}$ calculated using, respectively, steep and flat sources (coloured patches are at 1σ). Dashed lines are linear regressions (object number 4 is excluded). In the right-hand panel the comparison is with the [O III]-selected sample from H05.

Table 4. $\log(L_X/L_{[O\,III]})$ for uncorrected data.

Sample	$\log(L_X/L_{[O\,III]})$ (dex)	σ (dex)
H05 X-ray selected	2.15	0.51
H05 [O III] selected (type 1)	1.59	0.48
H05 [O III] selected (type 2)	0.57	1.06
This work	1.25	0.57

unobscured [O III]-selected AGN ($\log(L_X/L_{[O\,III]}) = 1.59$ dex, $\sigma = 0.48$ dex).

If we exclude the peculiar BL Lac object (number 4), the Kendall partial correlation test shows an unexpected, although not strong, correlation between [O III] and X-ray emissions with a significance of 99 per cent (92 per cent if we keep the BL Lac). This correlation is not present in the type 2 [O III]-selected sample of H05. A similar trend is instead present in the X-ray-selected sample, where X-ray absorption removes all the sources in the lower right part of the X-ray–[O III] plane, and in the type 1 objects in both the H05 samples, where obscuration is not important.

How can these difference be explained? The similarities between Seyfert 1 objects and our sample of LLAGN in the [O III]–X-ray plane suggest a lack or a reduced incidence of molecular/dusty structures (like the dusty torus present in Seyfert galaxies). The effect of such a structure would be to absorb X-ray emission coming from the inner part of the AGN. This is also confirmed by the X-ray spectral analysis, which does not find any sign of absorption in any source of the sample (apart from number 8, which is also the only HEG identified in the sample). The extinction-corrected [O III]–X-ray plane, shown in Fig. 4, is indeed similar to the uncorrected one, although due to the lack of high photon counts, our absorption-corrected data have big error bars.

From this analysis, we can conclude that, absorption being minimal, X-ray emission could be used as a good selection criteria for LEG sources at these low [O III] luminosities.

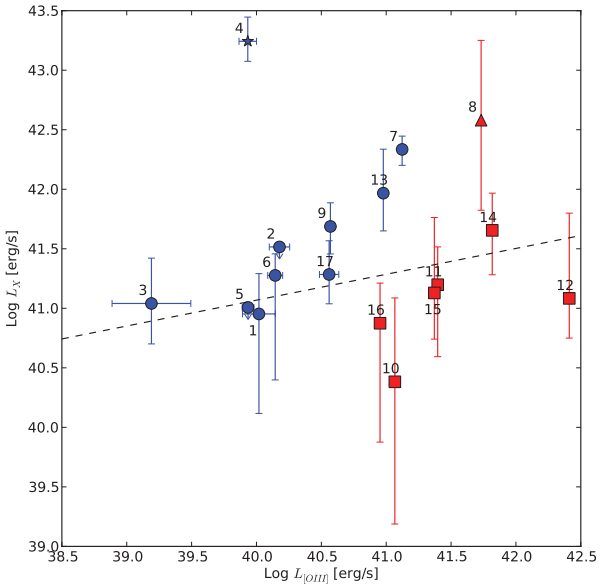

Figure 4. The same relation shown in Fig. 3 after correction for absorption both in [O III] and X-ray. Black line is the linear regression (object 4 excluded, slope: 0.22 ± 0.13, no evident correlation present as stated in Table 3). Symbols are as in Fig. 1.

4.2 The radio contribution

Our multiwavelength data set reveals another interesting fact. We find that a part of the scatter in the X-ray–[O III] relation can be directly linked to the radio spectra of the sources. Splitting the sample into radio steep-spectrum ($\alpha \geq 0.3$) and flat-spectrum ($\alpha < 0.3$) sources, we find that the two subsamples are still correlated in the [O III]–X-ray plane (at a significance level >99 per cent for flat-spectrum sources and of 95 per cent for steep-spectrum sources, see Table 3) and their linear fit slopes are compatible (flat: 0.91 ± 0.09; steep: 1.2 ± 0.5). However, the steep-spectrum sources are

systematically (∼1 order of magnitude) more [O III] luminous than flat-spectrum sources for a given X-ray luminosity. Radio emission spectrum thus plays a role in the location of the source in the $L_{[O\,III]}$–L_X plane, both for the dust-uncorrected (Fig. 3) and for the dust-corrected one (Fig. 4).

One possibility is that our flat-spectrum sources occur in a gas-poorer environment; consequently, their jets undergo a small interaction with the medium, so that, in the radio band, the very core of the AGN is the brightest part of the object. The flat spectrum is then explained as superimposition of many self-absorbed synchrotron spectra generated by the AGN core (Blandford & Konigl 1979). These sources will also have a fainter [O III] emission because there is less gas to ionize. This picture is reinforced by the fact that sources with steep spectrum show on average more dust extinction. In these sources [O III] flux is corrected for absorption (with the Balmer decrement method described in Section 3.3) by a factor of 17 ± 7 on average, while flat-spectrum sources have an average correction of a factor of 2.9 ± 0.8.

In the radio–X-ray plane (Fig. 5), there is no evident correlation between the two variables and the separation between steep- and flat-spectrum sources is not present any longer. However, sources of our sample classified as LEGs lie in the same location (with the important exception of source 7) found by Panessa et al. (2007) for a sample of low-luminosity radio galaxy (green line in Fig. 5) extracted from the FR I galaxies of the 3C catalogue (Balmaverde, Capetti & Grandi 2006). FR I galaxies are indeed almost always classified as LEGs, and Seyfert galaxies are usually 2–3 order of magnitude more powerful in X-ray for a given radio emission.

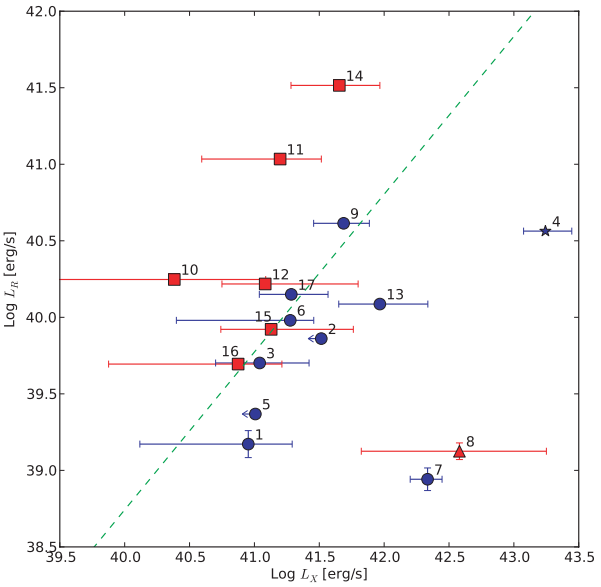

Figure 5. X-ray–radio (4 GHz) correlation. Green line is from a sample of low-luminosity radio galaxy (Panessa et al. 2007). Symbols are as in Fig. 1.

4.3 The Fundamental Plane of active black holes

Almost all sources of our sample lie above the Fundamental Plane of black hole activity described in Körding, Falcke & Corbel (2006) (Fig. 6, left-hand panel) and in M03 (Fig. 6, central panel). These two planes were derived using AGN selected with rather different criteria: for the first using only AGN where X-ray emission is believed to be jet dominated, while for the second explicitly excluding jet-dominated systems. An explanation of such a behaviour in terms of underestimating the X-ray extinction from the spectra and, therefore, a shift towards the left-hand side in Fig. 6 is unlikely. Even taking into account all difficulties in estimating the unabsorbed X-ray emission, the vast majority of our sources (14 out of 17) would need to be so heavily obscured as to bring their X-ray emission down by a factor of ∼100. Such a large fraction of heavily obscured objects would be very unusual, with current estimates of the incidence of Compton-thick AGN at these redshifts (albeit these are for somewhat higher luminosities) ranging between 20 and 50 per cent (see e.g. Goulding et al. 2011).

Also, the possibility of overestimating radio emission due to boosting effect appears improbable. A boosting effect should affect mainly sources with a flat spectrum, which is likely to be connected with emission from AGN core and jets, and would have affected both radio and X-ray emissions, while what we find is an excess of radio and a lack of X-ray emission. Furthermore, this would have brought forth a much larger scatter in the Fundamental Plane relation and the presence of some broadening in emission lines that are missing.

In fact, LEG sources in our sample describe a tighter relation (again with the exception of source 7) than what expected from the Fundamental Plane of M03. This relation has an intrinsic dispersion of $\sigma_\perp = 0.60$, while our LEG sample has a dispersion that is a factor of 1.7 smaller ($\sigma_\perp = 0.35$, which goes down to $\sigma_\perp = 0.26$ without source 7). The expected dispersion of the Fundamental Plane of Körding et al. (2006) ($\sigma_\perp = 0.28$) is instead compatible with what we find. It must also be noted that part of the dispersion in our data certainly arises from the errors associated to (at least) our very

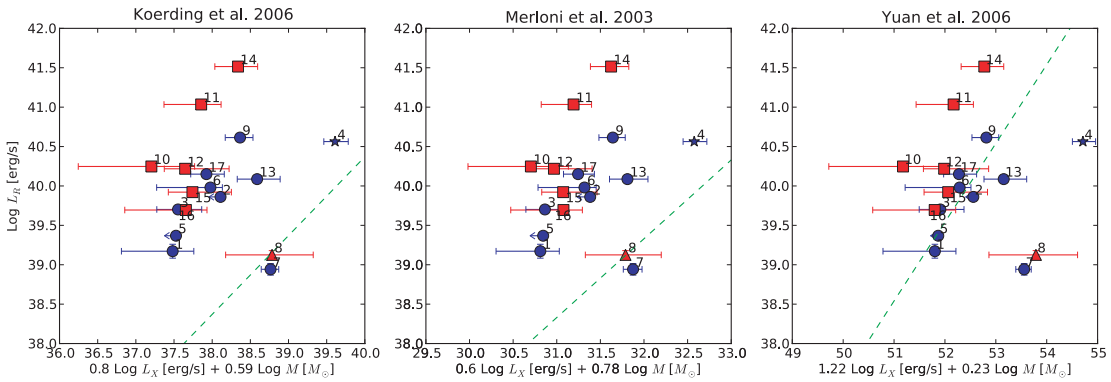

Figure 6. Fundamental Plane of active black hole relations. Green dashed lines shows the expected relation as found by Körding et al. (2006; left-hand panel), by M03 (central panel) and by Yuan et al. (2009; right-hand panel). Symbols are as in Fig. 1.

weak X-ray luminosities and consequent difficulties in estimating absorptions.

We find that neither M03 nor Körding et al. (2006) Fundamental Planes are able to correctly recover the relation between radio and X-ray emissions for our sample of LLAGN. This is indeed expected in the first case, where the majority of jet-dominated objects were excluded from the derivation. In the Körding et al. (2006) version of the Fundamental Plane relationship, only jet-dominated system (low-hard state XRB, LLAGN and FR I radio galaxies) instead were exploited for derivation; nevertheless, our data do not follow that relation either.

Similar results were found by Hardcastle et al. (2009); they tested the Fundamental Plane with a set of powerful radio galaxies from the 3CRR catalogue whose jet and accretion X-ray components can be disentangled using deep *XMM* spectroscopy. They found that, when considering only the accretion-related X-ray component, their sources lie in the predicted position on the Fundamental Plane of M03. Using the jet-related component instead, the sources move to the same location where our sample of low-luminosity objects lie. This underlines the care that needs to be taken before using Fundamental Plane relations with objects that could be jet dominated.

In Yuan & Cui (2005) an interpretation of the Fundamental Plane in terms of ADAF-jet model is given together with a prediction that the X-ray emission should originate from jets rather than ADAFs when the X-ray luminosity in the 2–10 keV band is lower than a critical value $L_{\rm X,crit}$ (equation 7 in Yuan & Cui 2005). In such a situation, the slope of the relation between radio and X-ray luminosity is steeper and the normalization is higher than that predicted by M03. Yuan, Yu & Ho (2009) tested these ideas with a sample of 22 LLAGN and found a relation very close to that defined by our sample (left-hand panel in Fig. 6) and close to the prediction of Yuan & Cui (2005) for X-ray emission produced at the base of the jet. However, the critical X-ray luminosity predicted by Yuan & Cui (2005), for the object in our sample, should correspond to $\log L_{\rm X,crit} \approx 39.6\,{\rm erg\,s^{-1}}$, while all our objects have higher X-ray luminosities. Nevertheless, it should be noted that the Yuan & Cui (2005) criterion is to be intended in a statistical sense and not as a sharp division between two populations, and the exact value of the critical luminosity may depend on the specific incarnation of the ADAF (viscosity, electron to ion heating efficiencies, etc.). Even so, the location of our sources in the radio luminosity–X-ray luminosity–SMBH mass space enhances the interpretation that X-ray emission in our sample (at least for LEG sources) is probably related to the jet synchrotron emission rather than the Comptonization emission from the (radiatively inefficient) accretion flow.

5 DISCUSSION

As we argued in Section 4.1, at least for LEG sources, the absence or a reduced incidence of dusty/molecular gas may explain the [O III]–X-ray correlation and the unusual missing signs of X-ray absorption in all LEG X-ray spectra (signs of absorption are only found in the HEG source). Moreover, part of the scatter in the observed [O III]–X-ray relations is directly linked to the radio spectra of the sources, and we have argued in Section 4.2 that our flat-spectrum sources live in a gas-poorer environment, and consequently their jets undergo a small interaction with the ambient medium.

Independent evidence for an intrinsic difference in the amount of cold/obscuring material in LLAGN has been gathered recently. Elitzur & Ho (2009) showed that, in a nearly complete sample of nearby AGN, the broad-line region (BLR) disappears at low intrinsic luminosities, and interpreted this fact within the disc-wind scenario for the BLR and toroidal obscuration in AGN (Elitzur 2008). If the BLR constitutes the inner, dust-free part of the cold molecular obscuring torus (see e.g. Netzer 2008), then a similar behaviour should be expected also for other indicators of intrinsic nuclear absorption. Indeed, Tran, Lyke & Mader (2011), using optical spectropolarimetry on a set of three low-luminosity type 2 AGN, found no sign of BLR, nor of obscuring torus. Furthermore, Burlon et al. (2010) found for the first time tantalizing evidence that the fraction of obscured AGN in a complete, hard X-ray-selected sample of nearby AGN, declines at $L_{\rm X} < 10^{42}\,{\rm erg\,s^{-1}}$.

In Section 4.3 we pointed out a different behaviour between LEG sources and those defining the M03 Fundamental Plane, and this is explainable with a different X-ray production mechanism between the population used to construct the Fundamental Plane and our sample. In the Fundamental Plane, X-ray emission is assumed to be generated by a (radiatively inefficient) accretion flow, while in LEG objects presented here, a much weaker (about 2 order of magnitude) X-ray emission could be generated by the jet itself. The tight correlation ($\sigma_\perp = 0.35$) between radio and X-ray emission for LEG objects enhances this conclusion, and is in agreement with the analysis of Yuan et al. (2009). Future studies on the relation between radio and X-ray emissions and the object mass in a bigger sample can unveil possible new relations similar to the Fundamental Plane but tuned for low-luminosity, jet-dominated objects. Based on the results presented here, such a plane will lie above the Fundamental Plane found in M03 and will have a smaller scatter as a consequence of the tight relation between radio and X-ray production in such kind of sources.

With respect to the analysis performed in M03, we remark here that the heterogeneity of their sample selection prevented any uniform classification of the X-ray spectra in terms of the amount of obscuration present. Based on the work presented here, it is likely that a large part of the scatter in the original Fundamental Plane relation could be due to the inclusion of both gas-poor and gas-rich sources in the original analysis.

Taken together, these considerations open the possibility to use X-ray emission as an unbiased estimator of source total power for LLAGN, provided robust indicators of a lack of cold gas in the observed systems is available. [O III] emission, although useful in the detecting and classification procedure, can be biased by the amount of dust present in the AGN surroundings, as we can infer from different positions of steep- and flat-spectrum sources in Fig. 4.

6 CONCLUSIONS

In this paper we analysed a set of sources extracted from the SDSS catalogue. For these sources we have measured *Chandra* X-ray flux, radio luminosity in two bands from the VLA and optical spectral information extracted from the SDSS data base. Our sources span a wide range in optical [O III] and radio luminosities, but they have very similar SMBH masses ($\sim 10^8\,{\rm M_\odot}$) and are all located over a narrow redshift range ($0.05 < z < 0.11$).

Although our sample spans a wide range of [O III] and radio luminosities, we found that 15 out of 17 sources are classified as LEGs. The sample shows a correlation on the uncorrected X-ray–[O III] luminosity plane that is not seen in samples of type 2 AGN with higher [O III] luminosity (H05). An absent or reduced obscuring torus can explain this relations, and different amount of gas in the AGN surroundings can account, to first order, for its scatter. This last property is well connected to the radio spectral index. This has important implications for selecting criteria in upcoming LLAGN surveys. For LEG samples, the lack of X-ray obscuration means

that X-ray emission can be used as a good selection quantity with no obscuration selection biases. Nevertheless, radio core emission is still the easiest way to identify this class of objects (Ho 2008), although more information (i.e. from optical spectra) is still required for object classification.

Summarizing, our conclusions are the following.

(i) At low luminosities ($L_X < 10^{42}\,\mathrm{erg\,s^{-1}}$) a selection criteria based on [O III] emission is not required in order to minimize the loss of obscured sources. At low luminosity, X-ray and [O III] emissions are correlated and there are no evident signs of X-ray absorption.

(ii) We found that all steep-spectrum sources have around an order of magnitude less [O III] emission than flat-spectrum sources with similar X-ray luminosity. We argue that the amount of ISM available for interaction in the proximity of the AGN is responsible for this distinction in the radio spectrum and for the difference in the production of the [O III] line.

(iii) In the radio–X-ray relation (and so in the Fundamental Plane of active black holes), LEG sources have a smaller dispersion and a reduced X-ray production compared to other types of AGN (i.e. Seyfert galaxies and quasars). This can be explained associating X-ray and radio production to the same physical mechanism, i.e. synchrotron emission from the base of the jet, in very good agreement with recent investigation (see e.g. Hardcastle et al. 2009) although obtained from sample selected with different criteria.

ACKNOWLEDGMENTS

We are grateful to Angela Bongiorno for her useful help and to ASTRON scientists, in particular John McKean, for their advice on the radio data reduction.

REFERENCES

Abazajian K. N. et al., 2009, ApJS, 182, 543
Akritas M. G., Siebert J., 1996, MNRAS, 278, 919
Avni Y., 1976, ApJ, 210, 642
Baldwin J. A., Phillips M. M., Terlevich R., 1981, PASP, 93, 5
Balmaverde B., Capetti A., Grandi P., 2006, A&A, 451, 35
Best P. N., Kauffmann G., Heckman T. M., Ivezić V., 2005, MNRAS, 362, 9
Best P. N., Kaiser C. R., Heckman T. M., Kauffmann G., 2006, MNRAS, 368, L67
Blandford R. D., Konigl A., 1979, ApJ, 232, 34
Broos P. S., Townsley L. K., Feigelson E. D., Getman K. V., Bauer F. E., Garmire G. P., 2010, ApJ, 714, 1582
Buckley J., James I., 1979, Biometrika, 66, 429
Burlon D., Ajello M., Greiner J., Comastri A., Merloni A., Gehrels N., 2010, ApJ, 728, 58
Buttiglione S., Celotti A., Capetti A., Dallacasa D., D'Odorico V., Giovannini G., 2009, Astron. Nachr., 330, 237
Cash W., 1979, ApJ, 228, 939
Charlot S., Fall S. M., 2000, ApJ, 539, 718
Chiaberge M., Capetti A., Celotti A., 2002, A&A, 394, 791
Dickey J. M., Lockman F. J., 1990, ARA&A, 28, 215
Elitzur M., 2008, New Astron. Rev., 52, 274
Elitzur M., Ho L. C., 2009, ApJ, 701, L91
Evans D. A., Worrall D. M., Hardcastle M. J., Kraft R. P., Birkinshaw M., 2006, ApJ, 642, 96
Falcke H., Biermann P. L., 1995, A&A, 293, 665
Falcke H., Koerding E., Markoff S., 2004, A&A, 414, 895
Freeman P., Doe S., Siemiginowska A., 2001, in Starck J.-L., Murtagh F. D., eds, Proc. SPIE Vol. 4477, Astronomical Data Analysis. SPIE, Bellingham, p. 76
Garmire G. P., Bautz M. W., Ford P. G., Nousek J. A., Ricker G. R., Jr, 2003, in Truemper J. E., Tananbaum H. D., eds, Proc. SPIE Vol. 4851, X-Ray and Gamma-Ray Telescopes and Instruments for Astronomy. SPIE, Bellingham, p. 28
Goulding A. D., Alexander D. M., Mullaney J. R., Gelbord J. M., Hickox R. C., Ward M., Watson M. G., 2011, MNRAS, 411, 1231
Hardcastle M. J., Evans D. A., Croston J. H., 2006, MNRAS, 370, 1893
Hardcastle M. J., Evans D. A., Croston J. H., 2009, MNRAS, 396, 1929
Heckman T. M., 1980, A&A, 87, 152
Heckman T. M., Kauffmann G., Brinchmann J., Charlot S., Tremonti C., White S. D. M., 2004, ApJ, 613, 109
Heckman T. M., Ptak A., Hornschemeier A., Kauffmann G., 2005, ApJ, 634, 161 (H05)
Heinz S., Sunyaev R. A., 2003, MNRAS, 343, L59
Hine R. G., Longair M. S., 1979, MNRAS, 188, 111
Ho L. C., 2002, ApJ, 564, 120
Ho L. C., 2008, ARA&A, 46, 475
Isobe T., Feigelson E., Nelson P., 1986, ApJ, 306, 490
Kaplan E., Meier P., 1958, J. Am. Stat. Assoc., 53, 457
Kewley L. J., Dopita M. A., Sutherland R. S., Heisler C. A., Trevena J., 2001, ApJ, 556, 121
Kewley L. J., Groves B., Kauffmann G., Heckman T., 2006, MNRAS, 372, 961
Körding E., Falcke H., Corbel S., 2006, A&A, 456, 439
Kraft R. P., Burrows D. N., Nousek J. A., 1991, ApJ, 374, 344
Laing R. A., Jenkins C. R., Wall J. V., Unger S. W., 1994, in Bicknell G. V., Dopita M. A., Quinn P. J., eds, ASP Conf. Ser. Vol. 54, The First Stromlo Symposium: The Physics of Active Galaxies. Astron. Soc. Pac., San Francisco, p. 201
Merloni A., Heinz S., Matteo T. D., Matteo D., 2003, MNRAS, 345, 1057 (M03)
Netzer H., 2008, New Astron. Rev., 52, 257
Nousek J. A., Shue D. R., 1989, ApJ, 342, 1207
Osterbrock D. E., 1989, Astrophysics of Gaseous Nebulae and Active Galactic Nuclei. University Science, Hill Valley
Panessa F., Barcons X., Bassani L., Cappi M., Carrera F., Ho L., Pellegrini S., 2007, A&A, 467, 519
Plotkin R. M., Anderson S. F., Hall P. B., Margon B., Voges W., Schneider D. P., Stinson G., York D. G., 2008, AJ, 135, 2453
Tran H. D., Lyke J. E., Mader J. A., 2011, ApJ, 726, L21
Tremaine S. et al., 2002, ApJ, 574, 740
Urry C. M., Padovani P., 1995, PASP, 107, 803
Veilleux S., Osterbrock D. E., 1987, ApJS, 63, 295
Whysong D., Antonucci R., 2004, ApJ, 602, 116
Yuan F., Cui W., 2005, ApJ, 629, 408
Yuan F., Yu Z., Ho L. C., 2009, ApJ, 703, 1034

This paper has been typeset from a TEX/LATEX file prepared by the author.